High-resolution optical spectroscopy of Tm^{3+} ions in $LiYF_4$: Crystal-field energies, hyperfine and deformation splittings, and the isotopic structure

S. A. Klimin,* D. S. Pytalev, and M. N. Popova
Institute of Spectroscopy, Russian Academy of Sciences, Troitsk, Moscow Region 142190, Russia

B. Z. Malkin, M. V. Vanyunin, and S. L. Korableva
Kazan State University, Kazan 420008, Russia

(Received 28 July 2009; revised manuscript received 10 November 2009; published 12 January 2010)

High-resolution optical Fourier spectroscopy was used to study the energies and widths of the crystal-field (CF) levels, hyperfine and deformation level splittings, and isotopic effects in the $LiYF_4:Tm^{3+}$ single crystals. We present the corrected sets of the CF levels and CF parameters for the Tm^{3+} ion in $LiYF_4$. The observed fine structure of spectral lines is shown to be caused by the hyperfine interaction, random lattice deformations, and isotopic disorder in the lithium sublattice. From a comparison between the observed and calculated fine structures we determine the characteristics of the random lattice deformations in highly diluted activated crystals and obtain an estimate of the fluorine displacements ($\sim 3\times 10^{-5}$ nm) in the nearest surrounding of the mass defect at the lithium site.

DOI: 10.1103/PhysRevB.81.045113 PACS number(s): 71.70.−d, 78.30.Hv, 78.40.Ha, 71.55.−i

I. INTRODUCTION

Recently, the Tm^{3+} ion was discussed in connection with quantum memory in rare-earth (RE) doped inorganic crystals.[1] Information can be stored in the two selectively populated long-living hyperfine sublevels of the Tm^{3+} ground state. Excitation and probing can be accomplished via the third level (a three-level Λ system) within reach of a narrow laser line. Such a scheme has been successfully realized in Tm^{3+}:yttrium aluminum garnet (YAG) under an external magnetic field, using a single mode stabilized-cavity semiconductor laser.[2] The ground state of the Tm^{3+} ions in YAG is an electronic singlet. The hyperfine interaction between the $4f$ electrons and the nuclear magnetic moment (the only thulium isotope ^{169}Tm has the nuclear spin $I=1/2$) results in the two degenerate electron-nuclear states. This degeneracy is lifted by the external magnetic field. The most evident shortcoming of this particular material, YAG, is the existence of six differently oriented Tm^{3+} centers that demonstrate different splittings under the action of the magnetic field. Even under the most favorable orientation of the magnetic field, at least 1/3 of the Tm^{3+} dopant ions are not involved in the quantum information processing.[2] Therefore, it is relevant to investigate Tm^{3+} doped crystals with magnetically equivalent positions for the RE ions. Among such crystals, the $LiYF_4$ crystal having the scheelite structure (the space group C_{4h}^6) is of special interest because, first, a broad experimental and theoretical information is available on the properties of this crystal that served as a model system for studying many phenomena and, second, $LiYF_4$ has excellent mechanical, thermal, and optical properties which is important for applications. For example, $LiYF_4:Tm^{3+}$ crystals are known as efficient media for multifrequency and upconversion lasers (see, e.g., Ref. 3).

In $LiYF_4$, the Tm^{3+} ions substitute for the Y^{3+} ions at the two magnetically equivalent positions with the S_4 point symmetry. In these positions, the electronic wave functions of RE ions with even number of electrons (as in the case of Tm^{3+}) transform according to the Γ_1 and Γ_2 nondegenerate and the Γ_{34} doubly degenerate irreducible representations of the S_4 point symmetry group. The ground state of Tm^{3+} in $LiYF_4$ has been identified as Γ_2, the next ones lying at 30 and 56 cm^{-1} higher are a Γ_{34} doublet and a Γ_1 singlet, respectively, separated by more than 200 cm^{-1} from other crystal-field (CF) sublevels of the $^3H_6$ ground multiplet.[3,4]

The energy levels of Tm^{3+} in $LiYF_4$ (derived from the analysis of the absorption and luminescence spectra registered at a rather poor spectral resolution of 1.5–4 cm^{-1}), the CF parameters and the magnetic g factors (derived from calculations) were first published in Ref. 4. Later, the optical spectra of $LiYF_4:Tm^{3+}$ were measured at a better resolution[3] and analyzed to get corrected sets of CF parameters and g factors.[3,5] The parameters of the electron-deformation interaction in the $LiYF_4:Tm^{3+}$ (1 at. %) crystal were determined from piezospectroscopic studies in Ref. 6. The nonlinear Zeeman and parastriction effects in the luminescence spectra of $LiY_{1-x}Tm_xF_4$ ($0.02\leq x\leq 1$) crystals were studied in Ref. 7. Surprisingly, the optical spectra of $LiYF_4:Tm^{3+}$ have never been published. The thermal broadening of several spectral lines of $LiYF_4:Tm^{3+}$ was measured in Ref. 8 to study electron-phonon interaction but any information on the low-temperature linewidths and shapes is absent.

The inhomogeneous width of the spectral lines in $LiYF_4:RE$ crystals is known to be as small as 0.007 cm^{-1} (Refs. 9 and 10) and even 0.0003 cm^{-1} in some special cases.[11] This fact offers a possibility to study the ion-lattice relaxation processes at low temperatures as well as a fine structure of spectral lines, using high-resolution optical spectroscopy. Earlier, we have performed high-resolution spectroscopic investigation of the hyperfine interaction and isotopic effects in $LiYF_4:Ho^{3+}$ (Refs. 9 and 12–14) and $LiYF_4:Er^{3+}$.[10,15] We also studied the electron-phonon interaction in $LiYF_4:Er^{3+}$, by comparing the measured low-temperature homogeneous linewidths and the calculated one-phonon relaxation rates.[15]

In this paper we present a detailed study of the high-resolution polarized temperature-dependent absorption spec-

tra of $LiYF_4:Tm^{3+}$ single crystals. We find the energies and symmetries of 41 CF levels and, where possible, measure their low-temperature widths and a fine structure. The CF parameters are corrected by fitting the results of calculations to our precise set of CF energies. The calculated magnetic g factors and hyperfine splittings are given and, when possible, compared with experimental data. We discuss manifestations of the random crystal fields and of isotopic disorder within the lithium sublattice. The preliminary experimental results of this work have been published in Refs. 16 and 17.

II. EXPERIMENTAL PROCEDURE

$LiYF_4$ crystals doped with Tm^{3+} (0.1, 0.5, 1, and 2 at. %) were grown by the Bridgman-Stockbarger method, as described in Ref. 10. We also used the holmium doped (0.1 at. % Ho^{3+}) samples of $^6Li_{0.07}{}^7Li_{0.93}YF_4$, $^6Li_{0.9}{}^7Li_{0.1}YF_4$, and of isotopically pure $^7LiYF_4$ with Tm^{3+} present as a trace impurity (at the level 0.2, 0.3, and 0.5 ppm, respectively). The thulium concentration was determined from integral intensities of the Tm^{3+} spectral lines. The spectra of Ho^{3+} and of Er^{3+} (present as a trace impurity) in these samples have been reported in our earlier works[9] and Ref. 10, correspondingly. The crystals were oriented by the x-ray diffraction method. Polarized high-resolution (up to 0.005 cm^{-1}) transmittance spectra were measured in a broad spectral (5000–23 000 cm^{-1}) and temperature (4.3–300 K) range using a Fourier spectrometer Bruker IFS 125HR and either a closed-cycle cryostat Cryomech ST 403 or a helium-vapor cryostat. The temperature was stabilized within ± 0.2 K. The absolute precision of the wave-number scale was 0.02–0.002 cm^{-1}, depending on the spectral resolution used. In contrast with high-resolution grating or tunable laser spectrometers, a Fourier-transform technique ensures an equally high resolution in a broad spectral range and a high absolute precision of the wave-number scale.

To obtain information on the level symmetry or on the electric dipole and the magnetic dipole contributions to the transition intensity, we registered all the spectra in the following three polarizations, α ($\boldsymbol{k} \| c; \boldsymbol{E}, \boldsymbol{H} \perp c$), σ ($\boldsymbol{k} \perp c; \boldsymbol{E} \perp c, \boldsymbol{H} \| c$), and π ($\boldsymbol{k} \perp c; \boldsymbol{E} \| c, \boldsymbol{H} \perp c$).

III. RESULTS AND DISCUSSION

A. Energies and symmetries of the Tm^{3+} crystal-field levels in $LiYF_4$

The electronic and spin-orbit interactions within the $4f^{12}$ configuration of the free Tm^{3+} ion result in many energy levels spread over approximately 37 500 cm^{-1}.[18] The first column of Table I lists the Tm^{3+} free-ion levels with energies less than 27 000 cm^{-1} and shows how they are split by the crystal field of the S_4 symmetry. For the free-ion levels, the LS coupling states $^{2S+1}L_J$ (Ref. 19) giving the largest contribution are indicated. As in the RE ions the LS coupling is not a good approximation, a considerable admixture of other LS states with the same value of J can take place. Thus, the Tm^{3+} free-ion level at about 5800 cm^{-1} has almost equal contributions of the $^3F_4$ and $^3H_4$ LS states[4,20] which leads to its different labeling, i.e., either $^3H_4$ (Ref. 18) or $^3F_4$.[3,4] Here we follow Refs. 3 and 4.

The spectra of all the measured multiplets are presented in Fig. 1. We have found that α- and σ-polarized absorption spectra of $LiYF_4:Tm^{3+}$ almost coincide for all multiplets except the $^3H_5$ one. Figures 1(b) and 1(a) demonstrate the spectra of this multiplet and, for a comparison, of the $^3F_4$ one in all the three studied polarizations, α, σ, and π. For all other multiplets only σ- and π-polarized spectra are presented [in Figs. 1(c)–1(f)]. It is easy to find from Table II summarizing the selection rules that a coincidence of the α and σ spectra announces a dominance of the electric dipole transitions. Thus, the electric dipole contribution dominates in the spectra of $LiYF_4:Tm^{3+}$, with the exception of the $^3H_6 \rightarrow {}^3H_5$ transition that is allowed as the magnetic dipole one in the free Tm^{3+} ion. In Fig. 1, the absorption spectra of $LiYF_4:Tm$ (0.1 at. %) are shown at the two temperatures, 4.3 and 70 K, together with spectral line identification. CF levels of the ground $^3H_6$ multiplet are numbered 1, 2, 3, etc., while those in each excited multiplet—A, B, C, etc., in the sequence of increasing energies.

On the example of Fig. 1(a) presenting the first excited multiplet $^3F_4$, we show how the application of the selection rules helps one to find the level symmetries not only for an excited multiplet but also for the ground-state multiplet. First, at low temperature when only the ground level is populated, we observe five spectral lines, three of them are π polarized while the rest two are σ (and α) polarized (we denote this fact as $3\pi+2\sigma$). Taking into account the selection rules for the electric dipole transitions (Table II) and the number of the CF levels of different symmetries for the S_4 site ($3\Gamma_1+2\Gamma_2+2\Gamma_{34}$, see the first column of Table I), we conclude that the ground state is Γ_2. If it were Γ_{34} or Γ_1, one would observe $2\pi+5\sigma$ or $2\pi+2\sigma$ lines, respectively, which is not the case. We also assign immediately the irreducible representations Γ_1 and Γ_{34} to the terminal levels for the π- and σ-polarized lines, respectively (see the second column of Table I). Because of our highly precise wave-number scale, we were able to set the correct sequence for the close levels 5756.5 cm^{-1} (Γ_{34}) and 5759.5 cm^{-1} (Γ_1) and to correct some data of Ref. 3 that basically agree rather well with our data. The remaining two $\Gamma_2 \rightarrow \Gamma_2$ transitions within the $^3H_6(1) \rightarrow {}^3F_4$ spectral multiplet are forbidden in the electric dipole approximation, they are absent in the low-temperature spectra. To find the energies of the Γ_2 levels, we raise the temperature and observe the spectral transitions from the excited CF sublevels of the ground multiplet. Again, using the selection rules of Table II, we find from the spectra at 70 K the lowest excited CF levels 29.8 cm^{-1} (Γ_{34}) and 55 cm^{-1} (Γ_1) and situate precisely the two Γ_2 levels of the $^3F_4$ multiplet at 5822.3 and 5966 cm^{-1} thus correcting the data of Refs. 3 and 4, by more than 20 cm^{-1} for the last figure. The high-frequency wing of the line 1G (5973 cm^{-1}) comes, probably, from vibronic transitions associated with other lower lying crystal-field levels. Indeed, the level G is separated by 374, 217, 214, and 151 cm^{-1}, respectively, from the four lowest levels in the $^3F_4$ multiplet. These frequencies correspond to an appreciable density of phonon states of the $LiYF_4$ lattice.[21]

Table I summarizes our experimental data on the energies, symmetries, and also low-temperature widths of the Tm^{3+}

TABLE I. Energies E, symmetries Γ, and half widths δE of the CF levels, g factors $g_{\|}$, and hyperfine splittings Δ_{HF} in $LiYF_4:Tm^{3+}$.

		Experiment		Theory		
Free-ion level and CF sublevels for S_4 site	Γ	E (cm^{-1})	δE (cm^{-1})	E (cm^{-1})	$g_{\|}$	Δ_{HF} (10^{-2} cm^{-1})
$^3H_6$, $3\Gamma_1+4\Gamma_2+3\Gamma_{34}$	2 (1)	0		0		
	34 (2)	29.8		29.4	0.494	0.268
	1 (3)	55		59.0		
	2 (4)	275		275.4		
	2 (5)	305		301.6		
	1 (6)			347.2		
	34 (7)	344		361.2	10.98	6.116
	34 (8)			395.2	3.506	1.968
	1 (9)			403.7		
	2 (10)			420.8		
$^3F_4$, $3\Gamma_1+2\Gamma_2+2\Gamma_{34}$	1 (A)	5598.8	0.011	5597.7		
	34 (B)	5756.5	1.8	5754.6	0.0324	0.022
	1 (C)	5759.5	1.33	5766.3		
	2 (D)	5822.3		5820.3		
	2 (E)	5966		5950		
	1 (F)	5968		5965.4		
	34(G)	5973	6.97	5971.3	4.508	2.637
$^3H_5$, $3\Gamma_1+2\Gamma_2+3\Gamma_{34}$	2 (A)	8283.6	0.008	8285.4		
	34(B)	8299	0.088	8301	0.151	0.065
	1 (C)	8319	1.05	8321		
	34(D)	8499.5	3.2	8503.5	10.09	7.276
	2 (E)	8511	4.07	8548.3		
	1 (F)	8518		8541.2		
	34(G)			8553.7	4.054	2.963
	1 (H)	8535		8564.2		
$^3H_4$, $3\Gamma_1+2\Gamma_2+2\Gamma_{34}$	2 (A)	12598		12600		
	1 (B)	12623	0.045	12622		
	34(C)	12643	0.088	12636	0.0736	0.019
	1 (D)	12744	2.8	12745		
	1 (E)			12801		
	34(F)	12834	2.89	12842	3.816	3.346
	2 (G)	12889		12916		
$^3F_3$, $\Gamma_1+2\Gamma_2+2\Gamma_{34}$	34(A)	14518	0.014	14511	4.644	2.829
	2 (B)	14546		14539		
	34(C)	14593	0.357	14584	0.505	0.019
	2 (D)	14595		14583		
	1 (E)	14605	0.313	14600		
$^3F_2$, $\Gamma_1+2\Gamma_2+\Gamma_{34}$	2 (A)	15093		15098		
	34(B)	15202	1.58	15198	1.256	1.991
	2 (C)			15231		
	1 (D)	15280[a]		15272		

CF levels in $LiYF_4$. As it has already been discussed in Ref. 4, because of the proximity of the actual S_4 symmetry space structure of the two first coordination shells of a RE ion in $LiYF_4$ to a higher D_{2d} symmetry structure, some spectral lines have very small intensities or are absent. At low temperatures, the lowest levels in the multiplets separated by a sufficiently wide energy gap from the lower lying multiplet are inhomogeneously broadened. This inhomogeneous

TABLE I. (*Continued.*)

Free-ion level and CF sublevels for S_4 site	Γ	Experiment E (cm^{-1})	Experiment δE (cm^{-1})	Theory E (cm^{-1})	Theory $g_\parallel$	Theory Δ_{HF} (10^{-2} cm^{-1})
$^1G_4$, $3\Gamma_1+2\Gamma_2+2\Gamma_{34}$	1 (A)	20970.5		20970		
	34(B)	21183	1.15	21176	0.294	0.230
	2 (C)	21267		21260		
	1 (D)	21296	8.98	21298		
	2 (E)	21507		21470		
	34(F)	21550	9.82	21531	4.126	3.415
	1 (G)	21560		21525		

[a]A very weak line at 15 250 cm^{-1} in σ polarization was used to determine the energy of the Γ_1(D) level.

broadening amounts to 0.008–0.014 cm^{-1}, the same as in $LiYF_4$:Ho and $LiYF_4$:Er crystals studied by some of us before.[9,10,15] (compare with the homogeneous linewidths of $10^{-6}/10^{-7}$ cm^{-1} as measured by two-pulse photon echoes for the lowest level in the $^3H_4$ multiplet in several Tm^{3+} doped crystals[22]). Higher lying levels in the multiplets are homogeneously broadened due to the ion—lattice relaxation processes.

B. Crystal-field calculations

The energy levels of Tm^{3+} in the S_4 symmetry crystal field in $LiYF_4$ can be calculated as eigenvalues of the Hamiltonian

$$H = H_{FI} + H_{CF} + H_{HF}. \quad (1)$$

Here H_{FI} is the free-ion Hamiltonian acting in the space of 91 states of the ground $4f^{12}$ configuration, defined by the Slater parameters $F^2=101\,576$, $F^4=71\,602$, and $F^6=50\,563$ cm^{-1} of the electrostatic interaction between the $4f$ electrons, the spin-orbit coupling constant $\xi=2630$ cm^{-1}, two-particle parameters $\alpha=17.26$, $\beta=-624$, and $\gamma=1820$ cm^{-1} of the electrostatic configuration interaction and parameters $P^2=650$, $P^4=300$, $P^6=70$ and $M^0=3.81$, $M^2=2.13$, $M^4=1.18$ cm^{-1} of correlated spin-orbit and spin-spin interactions, respectively.[23] The next term in Eq. (1),

$$H_{CF} = B_0^2C_0^2 + B_0^4C_0^4 + B_0^6C_0^6 + B_4^4(C_{-4}^4 + C_4^4) + iB_{-4}^4(C_{-4}^4 - C_4^4) + B_4^6(C_{-4}^6 + C_4^6) + iB_{-4}^6(C_{-4}^6 - C_4^6), \quad (2)$$

is the CF Hamiltonian (C_q^p are the electronic spherical tensor operators) represented in the crystallographic system of coordinates (with the z axis along the crystal c axis) by the seven real CF parameters B_k^p. Values of the CF parameters, $B_0^2=342$ (276), $B_0^4=-664$ (−616), $B_0^6=-72$ (−24), $B_4^4=-626.3$ (−612), $B_{-4}^4=-640.6$ (−658), $B_4^6=-484.6$ (−473), $B_{-4}^6=-352$ (−365) cm^{-1}, as well as of the free-ion Hamiltonian parameters presented above, were determined by variation in the results of calculations and of the literature data to get the best fit between the calculated and measured CF energies. In brackets, there are CF parameters calculated in the framework of the exchange charge model,[24] taking into account interactions of the $4f$ electrons with point charges of the lattice ions and with exchange charges defined by the squares of the overlap integrals of $4f(Tm^{3+})$ and $2s$, $2p(F^-)$ wave functions with the factors $G_s=G_\sigma=8.86$ and $G_\pi=6.23$ (see Ref. 24). The last term in Eq. (1),

$$H_{HF} = 2\mu_B\gamma_{Tm}\hbar\boldsymbol{I}\sum_k \frac{1}{r_k^3}\left[\boldsymbol{l}_k - \boldsymbol{s}_k + 3\frac{(\boldsymbol{s}_k\boldsymbol{r}_k)\boldsymbol{r}_k}{r_k^2}\right], \quad (3)$$

describes the magnetic dipole hyperfine interaction, here μ_B is the Bohr magneton, $\gamma_{Tm}=-2\pi\times 3.24$ MHz/T is the gyromagnetic ratio for the ^{169}Tm isotope (100% abundance),[25] $\boldsymbol{r}_k$ is the radius vector of the $4f$ electron with the orbital and spin moments $\boldsymbol{l}_k$ and $\boldsymbol{s}_k$, respectively. The matrix of Hamiltonian (1) was calculated in the basis of 182 electron-nuclear states and numerically diagonalized. The average value of r^{-3} for $4f$ electrons, $\langle r^{-3}\rangle=11.7$ atu, was taken from Ref. 26. The calculated energy levels, magnetic g factors $g_\parallel=2|\langle\Gamma_{34},\pm|\Sigma_k(l_{k,z}+2s_{k,z})|\Gamma_{34},\pm\rangle|$ (here $|\Gamma_{34},\pm\rangle$ are eigenfunctions of the z component of the magnetic dipole operator) and hyperfine splittings Δ_{HF} of Γ_{34} doublets are given in Table I. The calculated CF energies agree satisfactorily with the experimental data, the most remarkable differences between the measured and calculated CF energies of the upper sublevels of the $^1G_4$ multiplet are caused by a neglect of interactions between the ground and excited electronic configurations. It is worth noting that the hyperfine splitting of the ground multiplet calculated for a free ion ($\delta=0.08425$ cm^{-1}) agrees well with the value of the corresponding hyperfine constant $A(^3H_6)=-0.0132$ cm^{-1} presented in the literature[27] [$\delta=-6.5\cdot A(^3H_6)$].

C. Hyperfine and deformation splittings

It follows from Table I that the hyperfine splittings Δ_{HF} of the Γ_{34} energy levels of Tm^{3+} in $LiYF_4$ are rather small, they do not exceed several hundredths of wave number. To compare, Δ_{HF} for Ho^{3+} in $LiYF_4$ amount to 0.14–0.20 cm^{-1}.[12,13] As the ground state of Tm^{3+} in $LiYF_4$ is an electronic singlet (Γ_2) and, as it follows from calculations, the hyperfine splitting of the first excited Γ_{34} doublet is well within the inhomogeneously broadened spectral lines ($\Delta_{HF}<0.003$ cm^{-1}, see Table I), the search for a resolved hyperfine splittings is confined to the transitions from the ground singlet to the final

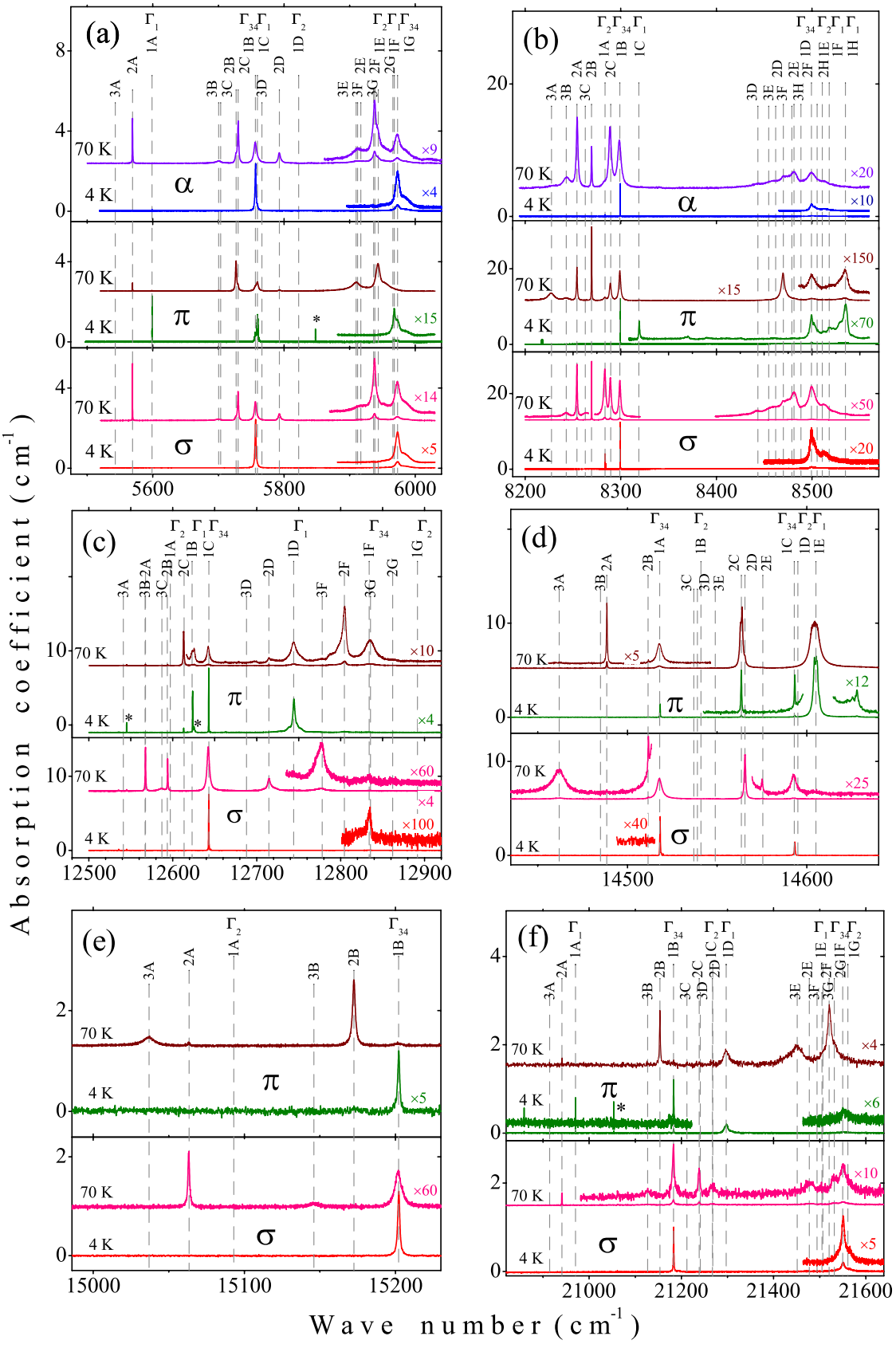

FIG. 1. (Color online) Absorption spectra of the (a) $^3F_4$, (b) $^3H_5$, (c) $^3H_4$, (d) $^3F_3$, (e) $^3F_2$, and (f) $^1G_4$ multiplets in $LiYF_4:Tm^{3+}$ at the temperatures 4.3 and 70 K for different polarizations of the incident light. In each figure, the sequence of icons from bottom to top corresponds to the σ, π, and α [shown for Figs. 1(a) and 1(b)] polarizations. Asterisks mark lines of some uncontrollable impurities.

TABLE II. Selection rules for optical transitions in S_4 site. Notations $d_i(\mu_i)$, $i=x,y$, or z refer to the components of electric (magnetic) dipole moment. Notations for the light polarization are explained in the text.

S_4	Γ_1	Γ_2	Γ_{34}
Γ_1	$\mu_z(\sigma_m)$	$d_z(\pi_e)$	d_x,d_y,μ_x,μ_y $(\alpha_e,\sigma_e;\alpha_m,\pi_m)$
Γ_2	$d_z(\pi_e)$	$\mu_z(\sigma_m)$	d_x,d_y,μ_x,μ_y $(\alpha_e,\sigma_e;\alpha_m,\pi_m)$
Γ_{34}	d_x,d_y,μ_x,μ_y $(\alpha_e,\sigma_e;\alpha_m,\pi_m)$	d_x,d_y,μ_x,μ_y $(\alpha_e,\sigma_e;\alpha_m,\pi_m)$	$d_z,\mu_z(\pi_e,\sigma_m)$

Γ_{34} states that are not too high from the lowest-energy level in a given multiplet and, thus, do not suffer from a relaxation broadening due to the electron-phonon interaction. Inspection of the energy levels together with their symmetries (Table I) delivers only two "candidates" for the observation of hyperfine splittings, namely, the lowest Γ_{34} level in the $^3F_3$ multiplet at 14 518 cm^{-1} and the Γ_{34} level at 8299 cm^{-1} that lies at 16 cm^{-1} above the lowest level in the $^3H_5$ multiplet. Figures 2 and 3 demonstrate resolved spectral doublets at both 14 518 and 8299 cm^{-1} in the absorption spectrum of the isotopically pure crystal $^7LiYF_4$:Ho (0.1 at. %) and Tm^{3+} (0.5 ppm) at 4.3 K. While the observed splitting of 0.039 cm^{-1} of the 14 518 cm^{-1} spectral line is in a reasonable agreement with results of calculations (see Table I), a drastic discrepancy is present for the line 8299 cm^{-1} (the measured splitting of this line 0.028 cm^{-1} is about 40 times larger that the calculated hyperfine splitting).

A reason for such an unexpectedly large splitting of the level 8299 cm^{-1} could lie in a different nature of the observed splitting, e.g., due to low-symmetry components of the crystal field induced by random lattice deformations. To check this idea, we have measured absorption spectra of $LiYF_4$:Tm^{3+} samples in different experimental conditions (Fig. 3). The narrowest lines and a clear splitting (0.028 cm^{-1}) of the level 8299 cm^{-1} were registered for a bulk sample with the trace impurity of thulium (data 1). Another sample, $LiYF_4$:Tm^{3+} (0.1 at. %), was subjected to mechanical treatment (cut and polished to the thickness of 90 μm). It was placed free into a helium vapor in the helium-vapor cryostat. The spectrum showed practically no splitting and the linewidth of 0.12 cm^{-1} (data 2). In these experimental conditions, neither a temperature gradient along the sample nor a mechanical stress due to different thermal expansion of the sample and of the sample holder were present but the lattice deformations could be induced by the cutting and polishing processes. When this same sample was glued along its perimeter to a cold finger of the closed-cycle cryostat, a line splitting up to 0.5 cm^{-1} appeared and each component of the split line was broadened to ~0.3 cm^{-1} (data 3). In this second case, a difference in the thermal expansion between the sample and the cold finger caused additional strains. These examples show qualitatively that the lattice deformations induced during the process of the sample preparation and/or its attachment to a mount can result in broadening and splitting of spectral lines that terminate at a non-Kramers doublet.

A non-Kramers Γ_{34} doublet splits under the lattice deformations of the Γ_2 symmetry determined by the deformation tensor components $e_1(\Gamma_2)=e_{xx}-e_{yy}$ and $e_2(\Gamma_2)=2e_{xy}$. In the crystallographic system of coordinates, the Hamiltonian of the electron-deformation interaction reads

$$H_{ed}=\sum_{\lambda=1,2} V_\lambda e_\lambda(\Gamma_2), \quad V_\lambda=\sum_{p,q} B^p_{q,\lambda} C^p_q. \tag{4}$$

The eight complex coupling constants $B^p_{q,\lambda}$ $[\lambda=1,2;\ B^p_{-q,\lambda}=(-1)^q B^{p*}_{q,\lambda}]$ were obtained earlier from piezospectroscopic

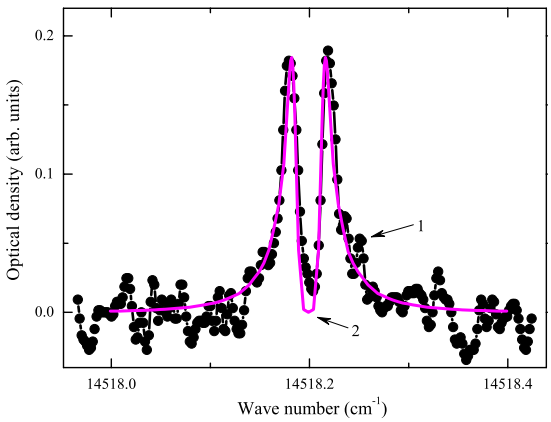

FIG. 2. (Color online) Measured (1) and calculated (2) line shapes for the transition $\Gamma_2(1,^3H_6)\rightarrow\Gamma_{34}(A,^3F_3)$ in the $^7LiYF_4$:Ho(0.1 at. %) sample containing Tm as trace impurity. $T=4.3$ K, σ polarization.

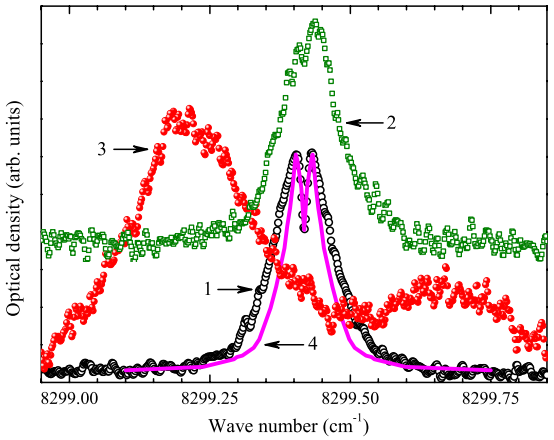

FIG. 3. (Color online) Measured (1–3) and calculated (4) line shapes for the transition $\Gamma_2(1,^3H_6)\rightarrow\Gamma_{34}(B,^3H_5)$ in the Tm^{3+} ion in $LiYF_4$ (π polarization, magnetic dipole transitions). (1)—the $^7LiYF_4$:Ho(0.1 at.%), Tm (0.5ppm) bulk sample (8.8 mm), (2)—the $^7Li_{0.93}$ $^6Li_{0.07}YF_4$:Tm (0.1 at. %) sample (90 μm) placed free into a helium vapor in the helium-vapor cryostat, and (3)—the sample (2) but glued along its perimeter to a mount. $T=4.3$ K.

measurements:[6,28] $B^2_{2,1}=1.63-1.76i$, $B^4_{2,1}=-1.04-2.84i$, $B^6_{2,1}=-0.34+0.48i$, $B^6_{6,1}=-0.79+0.94i$, $B^2_{2,2}=3.2+0.58i$, $B^4_{2,2}=-2.72-2.05i$, $B^6_{2,2}=-0.9+1.08i$, and $B^6_{6,2}=-1.4+1.73i$ (10^3 cm^{-1}). Using the perturbation theory, we derive the following expression for energies of the sublevels of a fixed Γ_{34} doublet split by the hyperfine and electron-deformation interactions:

$$\hbar\omega_{\pm}(e_1,e_2) = E(\Gamma_{34}) \pm [(\Delta_{HF}/2)^2 + |v_1e_1 + v_2e_2|^2]^{1/2}, \tag{5}$$

where $v_\lambda=\langle\Gamma_{34},+|V_\lambda|\Gamma_{34},-\rangle$ and $E(\Gamma_{34})$ is the corresponding eigenvalue of the Hamiltonian $H_{FI}+H_{CF}$. The spectral distribution of the absorption is given by a convolution

$$I(\omega) = \int\int \{S[\omega-\omega_-(e_1,e_2)] + S[\omega-\omega_+(e_1,e_2)]\}g(e_1,e_2)de_1de_2, \tag{6}$$

where $g(e_1,e_2)$ is the distribution function of lattice deformations and $S(\omega)$ is the spectrometer shape function. We assume $S(\omega)$ to be a Gaussian with the dispersion of 0.0035 cm^{-1}. In the framework of an elastic isotropic continuum approximation and in the case of low concentration of lattice defects, the distribution function of lattice deformations has the following form:[29]

$$g(e_1,e_2) = \frac{\Gamma}{2\pi}(e_1^2+e_2^2+\Gamma^2)^{-3/2}, \tag{7}$$

where the width Γ is proportional to the concentration of the point lattice defects. We used the distribution [Eq. (7)] to simulate the line shapes for the transitions $\Gamma_2(1,{}^3H_6)\rightarrow\Gamma_{34}(B,{}^3H_5)$ and $\Gamma_2(1,{}^3H_6)\rightarrow\Gamma_{34}(A,{}^3F_3)$ in the isotopically pure sample $^7LiYF_4$ considering the width Γ as a fitting parameter. As it is seen in Figs. 2 and 3, where the results of simulations are compared to the measured spectrum, both resolved spectral doublets are well reproduced when using the same width $\Gamma=8.5\times10^{-5}$. The doublet $\Gamma_{34}(B,{}^3H_5)$ at 8299 cm^{-1} is strongly affected by internal residual strains ($v_1=567-604i$, $v_2=420-387i$ cm^{-1}) and its splitting is caused entirely by the random crystal fields. From the observed splitting ~0.5 cm^{-1} of this doublet at the liquid-helium temperature in the glued sample $LiYF_4$:Tm (0.1 at. %) (data 3 in Fig. 3), it follows that internal strains induced by the inhomogeneous lattice contraction are in the range 8–28 MPa. The deformation potentials of the $\Gamma_{34}(A,{}^3F_3)$ doublet at 14 518 cm^{-1} are about three to four times less ($v_1=145+182i$, $v_2=166+138i$ cm^{-1}) and its splitting increases only by 38% due to random strains in the $^7LiYF_4$ sample (up to 0.039 cm^{-1} as compared to theoretical value $\Delta_{HF}=0.0283$ cm^{-1}).

D. Isotopic structure in optical spectra of $LiYF_4$:Tm^{3+}

Earlier, a specific fine structure in the optical and electron paramagnetic resonance spectra of Ho^{3+} and Er^{3+} ions due to isotopic disorder in the lithium sublattice of the $LiYF_4$ host matrix was observed.[9,10,30] It was shown that this structure is mainly caused by the dependence of the static crystal field

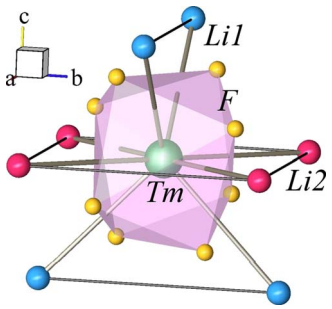

FIG. 4. (Color online) Fragment of the $LiYF_4$:Tm lattice structure.

for a given impurity RE ion on the lithium isotopic composition in the nearest neighborhood. Each RE^{3+} ion (placed at the origin of the crystallographic system of coordinates) has four nearest Li^+ ions (Li1) in the vertexes ($\pm a/2$ 0 $c/4$), (0 $\pm a/2$ $-c/4$) of a tetrahedron at the distance 0.3824 nm and four next-nearest Li^+ ions (Li2) in the corners of a square ($\pm a/2$ $\pm a/2$ 0) at the slightly different distance 0.3853 nm (a and c are the lattice constants, see Fig. 4). The probability to find n_1 isotopes ^{6}Li in the first position and n_2 isotopes ^{6}Li in the second one in the sample $^6Li_x{}^7Li_{1-x}YF_4$ is given by the formula

$$P_{n_1n_2} = C_4^{n_1}C_4^{n_2}x^{n_1+n_2}(1-x)^{8-(n_1+n_2)}, \tag{8}$$

where $C_4^{n_i}$ are the binomial coefficients.

In the case of small concentration x of ^{6}Li (or $1-x$ of ^{7}Li), isotopes ^{6}Li (^{7}Li) can be considered as isolated mass defects. A mass defect perturbs the lattice structure at low temperatures due to anharmonic character of lattice vibrations. The first coordination shell (four fluorine ions) of the light ^{6}Li isotope expands.[31] Displacements of the fluorine ions from equilibrium positions in the perfect-crystal lattice bring about shifts of CF energy levels of impurity RE ions. The largest shifts in the spectrum of a RE ion are induced by the nearest-neighbor fluorine ions that push off from the mass defects in the Li1 and Li2 positions.

The observed spectrum can be simulated as a superposition

$$I(\omega) = \sum_{n_1n_2} S(\omega-\omega_{n_1n_2})P_{n_1n_2} \tag{9}$$

of spectral lines with frequencies $\omega_{n_1n_2}=\omega_0+n_1\Delta\omega_{10}+n_2\Delta\omega_{01}$, where $\Delta\omega_{10}$ and $\Delta\omega_{01}$ are the changes of the transition frequency ω_0 in the perfect lattice due to a single mass defect in the Li1 or Li2 positions, respectively.

In the absorption spectra of $LiYF_4$:Tm^{3+} samples, only the most narrow spectral lines exhibit resolved isotopic structure. Figure 5 shows a fine structure within the singlet-to-singlet $\Gamma_2(1,{}^3H_6)\rightarrow\Gamma_1(A,{}^3F_4)$ spectral line in the $^6Li_x{}^7Li_{1-x}YF_4$:Tm^{3+} (0.1 at. %, $x=0.0742$) crystal with natural abundance of lithium isotopes. The observed structure is reasonably explained by isotopic disorder in the neighborhood of the Tm^{3+} site. This particular line presents an example when the spectral components connected with ^{6}Li isotopes in the Li1 and Li2 positions are shifted in op-

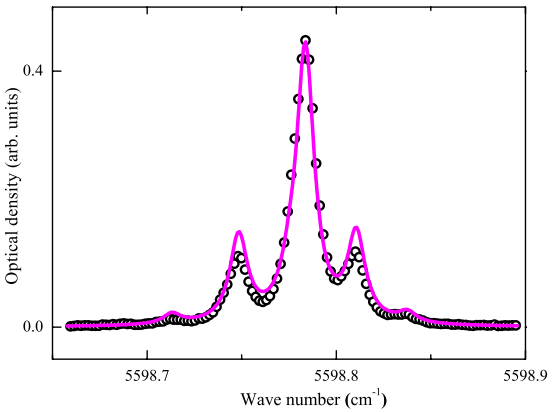

FIG. 5. (Color online) Measured (symbols) and simulated (solid curve, $\Delta\omega_{01}=0.0269$ cm^{-1}, $\Delta\omega_{10}=-0.0353$ cm^{-1}) isotopic structure of the transition $\Gamma_2(1,{}^3H_6)\rightarrow\Gamma_1(A,{}^3F_4)$ in the $LiYF_4:Tm^{3+}$ (0.1 at. %) sample (π polarization) with the natural abundance of lithium isotopes ^{7}Li (92.58%) and ^{6}Li (7.42%).

posite directions from the main line. Figure 6 gives another example of the isotopic structure and a direct evidence of the origin of this structure. The spectral line corresponding to the magnetic dipole transition $\Gamma_2(1,{}^3H_6)\rightarrow\Gamma_2(A,{}^3H_5)$ does not exhibit any structure in the isotopically enriched sample $^7LiYF_4$ [see Fig. 6(b)]. However, in the samples $^7Li_{1-x}{}^6Li_xYF_4$ containing mass defects of different signs in the lithium sublattice, $\Delta m=-1$ for $x=0.0742$ [Fig. 6(a)] and $\Delta m=+1$ for $x=0.9$ [Fig. 6(c)], well-resolved satellites shifted in different directions from the main line are observed.

The data of measurements can be used to estimate the displacement vector $\Delta\boldsymbol{R}$ of the fluorine ions in the first coordination shell of a mass defect in lithium sites. Derivatives of the CF parameters in respect to the $\Delta\boldsymbol{R}$ components were computed in the framework of the exchange charge model approbated by calculations of the CF energies (see Sec. III B above). Next, the $\Delta\boldsymbol{R}$ components were considered as fitting parameters in the simulations of spectral envelopes, Eq. (9). Rather good agreement between the simulated and measured spectra was achieved when using the displacement vector $\Delta\boldsymbol{R}=(-0.331,-0.247,0.061)\times10^{-4}$ nm of the fluorine ion with coordinates (0.146, 0.085, and 0.087) nm relative to the unit mass defect ($\Delta m=+1$) in the lithium site (see Figs. 5 and 6). Displacements of the other three nearest-neighbor fluorine ions can be easily obtained by S_4 symmetry operations. The calculated intervals in the isotopic structures of the $\Gamma_2(1,{}^3H_6)\rightarrow\Gamma_1(A,{}^3F_4)$ and $\Gamma_2(1,{}^3H_6)\rightarrow\Gamma_2(A,{}^3H_5)$ transitions are presented in the figure captions.

It should be noted that the simulated envelope in Fig. 6(c) corresponds to the concentration $x=0.82$ instead the nominal $x=0.9$. The obtained displacement vector agrees qualitatively with the results of calculations [$\Delta\boldsymbol{R}=(-0.324,-0.098,-0.014)\times10^{-4}$ nm at 4.2 K] based on the rigid-ion model of $LiYF_4$ lattice dynamics.[21,31]

The isotopic structure was also observed within the singlet-to-doublet transition $\Gamma_2(1,{}^3H_6)\rightarrow\Gamma_{34}(A,{}^3F_3)$ in the $LiYF_4:Tm^{3+}$ (0.1 at. %) sample with the natural abundance of lithium isotopes. The calculated shifts of the satellites $\Delta\omega_{01}=0.0225$ cm^{-1} and $\Delta\omega_{10}=0.008$ cm^{-1} from the main

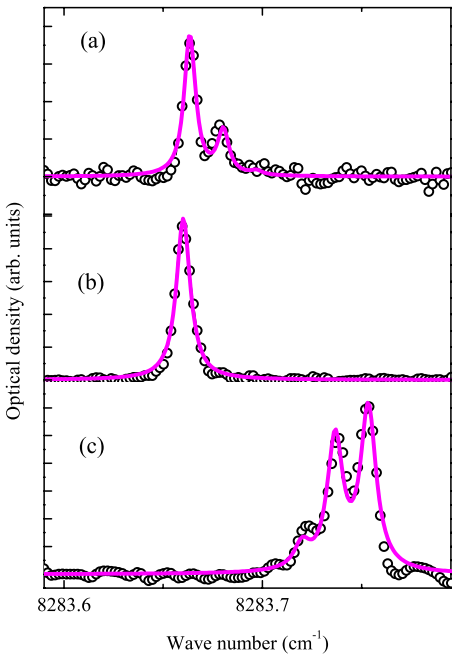

FIG. 6. (Color online) Measured (symbols) and simulated (solid curves) spectral lines corresponding to the transition $\Gamma_2(1,{}^3H_6)\rightarrow\Gamma_2(A,{}^3H_5)$ of the Tm^{3+} ions (σ polarization) in the $^6Li_x{}^7Li_{1-x}YF_4$ samples with different isotopic composition in the lithium sublattice: (a) $x=0.0742$, $\Delta\omega_{01}=0.016$ cm^{-1}, and $\Delta\omega_{10}=0$; (b) $x=0$; and (c) $x=0.9$, $\Delta\omega_{01}=-0.016$ cm^{-1}, and $\Delta\omega_{10}=0$.

lines agree satisfactorily with the measured shape of the spectrum.

IV. CONCLUSIONS

The temperature-dependent polarized optical-absorption spectra of the $LiYF_4:Tm^{3+}$ single crystals were studied by high-resolution Fourier spectroscopy. Several important corrections were introduced into the previously established[3] scheme of the crystal-field energy levels. This precise set of CF energies was used to correct the CF parameters. Experimental data on the low-temperature linewidths are presented. The inhomogeneous broadening is on the order of 0.01 cm^{-1}. Fine structure of the spectral lines was observed and analyzed using the results of our CF calculations. It was shown that the observed splitting (0.028 cm^{-1}) of the Γ_{34} doublet at 8299 cm^{-1} is caused by random lattice deformations while the dominant contribution to the splitting (0.039 cm^{-1}) of the 14 518 cm^{-1} doublet comes from the hyperfine interaction. Simulation of the observed doublet line shapes enabled us to determine the characteristics of the random lattice deformations in highly diluted activated crystals and to estimate internal strains induced by the inhomogeneous lattice contraction for a sample glued along its perimeter to a cold finger of a cryostat (8–28 MPa). Isotopic structure of the spectral lines due to the ^{7}Li-^{6}Li isotopic disorder in the neighborhood of the Tm^{3+} site was found and simulated in the framework of the exchange charge model approbated by calculations of the CF energies. This gave an estimate of the fluorine displacements ($\sim3\times10^{-5}$ nm) in the

nearest surrounding of the mass defect at the lithium site.

ACKNOWLEDGMENTS

The authors are grateful to M. A. Petrova for the growth of isotopically enriched crystals and to T. C. Ozawa and Sung J. Kang for the program "Balls & Sticks" (Ref. 32) we have used for drawing Fig. 4. Financial support from the Russian Foundation for Basic Research (Grants No. 09-02-01067 and No. 09-02-00930) and from the Russian Academy of Sciences under the Programs for Basic Research is acknowledged.

*klimin@isan.troitsk.ru

[1] O. Guillot-Noël, Ph. Goldner, E. Antic-Fidancev, and J.-L. Le Gouët, Phys. Rev. B **71**, 174409 (2005).
[2] F. de Seze, A. Louchet, V. Crozatier, I. Lorgere, F. Bretenaker, J.-L. Gouët, O. Guillot-Noël, and Ph. Goldner, Phys. Rev. B **73**, 085112 (2006).
[3] M. Dulick, G. E. Faulkner, N. J. Cockroft, and D. C. Nguyen, J. Lumin. **48-49**, 517 (1991).
[4] H. P. Jenssen, A. Linz, R. P. Leavitt, C. A. Morrison, and D. E. Wortman, Phys. Rev. B **11**, 92 (1975).
[5] X. Chen and Z. Luo, J. Phys.: Condens. Matter **9**, 4197 (1997).
[6] A. V. Vinokurov, B. Z. Malkin, A. I. Pominov, and A. L. Stolov, Sov. Phys.-Solid State **28**, 211 (1986).
[7] R. Yu. Abdulsabirov, A. A. Kazantsev, S. L. Korableva, B. Z. Malkin, S. I. Nikitin, and A. L. Stolov, J. Lumin. **117**, 225 (2006).
[8] A. Ellens, H. Andres, M. L. H. ter Heerdt, R. T. Wegh, A. Meijerink, and G. Blasse, Phys. Rev. B **55**, 180 (1997).
[9] N. I. Agladze, M. N. Popova, G. N. Zhizhin, V. J. Egorov, and M. A. Petrova, Phys. Rev. Lett. **66**, 477 (1991).
[10] E. P. Chukalina, M. N. Popova, S. L. Korableva, and R. Yu. Abdulsabirov, Phys. Lett. A **269**, 348 (2000).
[11] R. M. Macfarlane, R. M. Meltzer, and B. Z. Malkin, Phys. Rev. B **58**, 5692 (1998).
[12] N. I. Agladze and M. N. Popova, Solid State Commun. **55**, 1097 (1985).
[13] N. I. Agladze, E. A. Vinogradov, and M. N. Popova, Sov. Phys. JETP **64**, 716 (1986).
[14] M. N. Popova and N. I. Agladze, Mol. Phys. **102**, 1315 (2004).
[15] M. N. Popova, E. P. Chukalina, B. Z. Malkin, and S. K. Saikin, Phys. Rev. B **61**, 7421 (2000).
[16] D. S. Pytalev, S. A. Klimin, and M. N. Popova, Phys. Lett. A **372**, 3506 (2008).
[17] S. A. Klimin and D. S. Pytalev, J. Rare Earths **27**, 633 (2009).
[18] G. H. Dieke, *Spectra and Energy Levels of Rare Earth Ions in Crystals* (Interscience, New York, 1968).
[19] Here S and J are the values of the spin and the total angular momentum, respectively, letters S, P, D, F, etc., correspond to the values of the orbital momentum 0, 1, 2, 3, etc.
[20] H. P. Christensen, Phys. Rev. B **19**, 6573 (1979).
[21] S. Salaun, A. Bulou, M. Rousseau, B. Hennion, and J. Y. Gesland, J. Phys.: Condens. Matter **9**, 6957 (1997).
[22] R. M. Macfarlane, J. Lumin. **100**, 1 (2002).
[23] H. M. Crosswhite and H. Crosswhite, J. Opt. Soc. Am. B **1**, 246 (1984).
[24] B. Z. Malkin, in *Spectroscopy of Solids Containing Rare-Earth Ions*, edited by A. A. Kaplyanskii and R. M. Macfarlane (Elsevier Science, Amsterdam, 1987), p. 13.
[25] M. A. H. McCausland and I. S. Mackenzie, Adv. Phys. **28**, 305 (1979).
[26] R. E. Watson and A. J. Freeman, in *Hyperfine Interactions*, edited by A. J. Freeman and R. B. Frankel (Academic, New York, London, 1967).
[27] A. Abragam and B. Bleaney, *Electron Paramagnetic Resonance of Transition Ions* (Oxford University Press, Oxford, 1970).
[28] L. K. Aminov and B. Z. Malkin, *Dynamics and Kinetics of Electronic and Spin Excitations in Paramagnetic Crystals* (Kazan State University Press, Kazan, 2008).
[29] M. A. Ivanov, V. Ya. Mitrofanov, L. D. Falkovskaya, and A. Ya. Fishman, J. Magn. Magn. Mater. **36**, 26 (1983).
[30] G. S. Shakurov, B. Z. Malkin, M. V. Vanyunin, and S. L. Korableva, Phys. Solid State **50**, 1619 (2008).
[31] B. Z. Malkin and S. K. Saikin, Proceedings of the Tenth Feofilov Symposium on Spectroscopy of Crystals Activated by Rare-Earth and Transitional-Metal Ions, edited by Alexander I. Ryskin and Vadim F. Masterov [Proc. SPIE **2706**, 193 (1996)].
[32] T. C. Ozawa and Sung J. Kang, J. Appl. Crystallogr. **37**, 679 (2004).